

## Nanopatterning of multiferroic BiFeO<sub>3</sub> using “soft” electron beam lithography

Tao Sun,<sup>a)</sup> Zixiao Pan, and Vinayak P. Dravid<sup>b)</sup>

*Department of Materials Science and Engineering, International Institute of Nanotechnology, Northwestern University, Evanston, Illinois 60208*

Zhaoyu Wang and Min-Feng Yu

*Department of Mechanical and Industrial Engineering, University of Illinois at Urban-Champaign, Urbana, Illinois 61801*

Jin Wang

*Advanced Photon Source, Argonne National Laboratory, Argonne, Illinois 60439*

(Received 8 August 2006; accepted 1 September 2006; published online 18 October 2006)

The authors report fabrication of multiferroic BiFeO<sub>3</sub> (BFO) by the soft electron beam lithography technique. BiFeO<sub>3</sub> nanopatterns with less than 100 nm characteristic dimension are fabricated from its liquid-phase precursor on diverse substrates. The chemical constituents and phase purity are characterized by transmission electron microscopy. The ferroelectric behavior is confirmed by piezoresponse force microscopy. A saturation magnetization of about 10 emu/cm<sup>3</sup> is observed, demonstrating the multiferroic characteristic of the BFO nanopatterns. Furthermore, the BFO nanolines patterned on SrTiO<sub>3</sub> substrate exhibit a bambolike structure, which can serve as an excellent model system for investigating the contribution of grain boundaries to the leakage current. © 2006 American Institute of Physics. [DOI: 10.1063/1.2364117]

Ordered low-dimensional, multifunctional materials have attracted considerable attention from the viewpoint of fundamental mechanism of size-dependent properties as well as their promise in high-performance devices.<sup>1,2</sup> In this context, multiferroic materials belong to the class of intriguing emerging functional materials, not only because of the coexistence of spontaneous polarization and magnetization in a single compound but also for the synergistic coupling between these functionalities.<sup>3-5</sup> The interaction between electric and magnetic orderings can potentially allow for manipulation of both charge and spin by applying a single homogeneous electric or magnetic field. Therefore, more freedom is allowed for designing related devices, such as access memory in which data recorded by electric field could be read nondestructively via magnetization.

BiFeO<sub>3</sub>, a rhombohedrally distorted perovskite, has long been known as a multiferroic material with ferroelectric ( $T_C \sim 1103$  K) and  $G$ -type antiferromagnetic ( $T_N \sim 643$  K) properties.<sup>6,7</sup> Its unique feature of exhibiting both orders at room temperature is highly favorable for applications. Recently, a large ferroelectric polarization, comparable to the prototypical Pb(Zr<sub>x</sub>Ti<sub>1-x</sub>)O<sub>3</sub>, was reported for epitaxial BiFeO<sub>3</sub> (BFO) thin films, making it a promising alternative for lead-free ferroelectrics used for nonvolatile random-access memory.<sup>8,9</sup> Although it is believed that the decrease of oxygen vacancy is the origin for the significant ferroelectric property enhancement of BFO that occurred from bulk to thin-film form,<sup>8,10</sup> crystal structure change due to the reduced dimension cannot be ignored and deserves further investigation. Therefore, fabrication of BFO nanostructures will greatly expand the scope for investigating dimensional influence on material properties. On the other hand, for ferroelectric materials, the clamping effect imposed by the substrate is

greatly reduced in three-dimensional (3D) nanostructure compared with thin film. It was demonstrated that this effectively facilitated the movement of ferroelastic walls, thereby enhancing the piezoelectric coefficient.<sup>11,12</sup> It is highly desirable to develop a unique patterning approach to achieve well-defined dimensions and separation of BFO nanoelements. However, fabrication of low-dimensional BFO nanostructures, especially substrate-base nanopatterns with well-defined size and separation, still remains a challenge and has not been thoroughly studied.<sup>13,14</sup>

We have recently introduced a facile patterning technique termed “soft electron beam lithography” (soft-eBL) for site-specific fabrication of solid-state nanostructures. The soft-eBL shows high versatility for patterning two-dimensional planar elements as well as 3D hierarchical features.<sup>15,16</sup> In this letter, we report fabrication of BFO nanopatterns using the soft-eBL technique as well as their extensive characterization and validation of their functional behavior.

The soft-eBL technique as a combination of electron beam lithography and spinning of sol-gel precursors for patterning the ceramic nanostructures has been previously reported by our group.<sup>15,16</sup> In this work, the sol-gel precursor of BFO for soft-eBL was prepared by dissolving Bi(III) acetate and Fe(III) acetylacetonate into the solution of acetic acid and de-ionized water and stirring at 50 °C for 3 h. An excess amount of Bi<sup>3+</sup> source (2 mol % ratio) was added to compensate for the loss of Bi during annealing. By using an x-ray diffractometer (ATX-G, Rigaku, Japan), grazing incidence x-ray diffraction (GIXRD) was carried out to investigate the phase purity of the sol-gel prepared BFO thin film (considering the small amount of materials in the nanopatterns). The XRD results indicate that the BFO thin film is in a pure phase after the heat treatment. The details of fabrication of BFO thin films and GIXRD characterization are described in the supplementary material.

<sup>a)</sup>Also at Advanced Photon Source, Argonne National Laboratory, Argonne, IL 60439.

<sup>b)</sup>Electronic mail: v-dravid@northwestern.edu

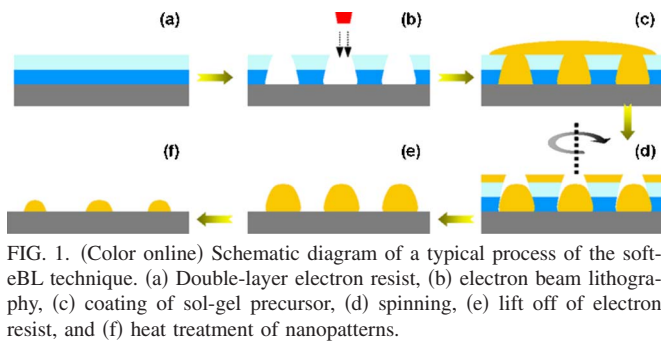


FIG. 1. (Color online) Schematic diagram of a typical process of the soft-eBL technique. (a) Double-layer electron resist, (b) electron beam lithography, (c) coating of sol-gel precursor, (d) spinning, (e) lift off of electron resist, and (f) heat treatment of nanopatterns.

Figure 1 schematically illustrates the soft-eBL process. Methyl methacrylate (MMA)–methacrylic acid (MAA) copolymer and polymethyl methacrylate (PMMA) were spun on substrates sequentially as electron beam resist. Since MMA-MAA copolymer is more sensitive to the electron beam, it effectively helps complete lift off. Electron beam lithography (Quanta 600F, FEI Company, USA) was carried out to pattern arrays of disks or lines on the resist. After developing, BFO sol was spun on the substrate followed immediately by drying at 150 °C to gelate the sol. The samples were then soaked in acetone to lift off the electron beam resist, as well as excess BFO, from the unpatterned area. Crystalline BFO patterns were obtained after annealing at 600 °C for 30 min.

The morphology of the patterns was investigated with scanning electron microscopy (SEM) (Quanta 600F, FEI Company, USA) and atomic force microscopy (AFM) (Nanoscope III microscope, Digital Instruments, USA). A series of SEM images of BFO nanopatterns is shown in Fig. 2. Figure 2(a) shows BFO nanodots of 220 nm in diameter on a Si wafer. Figure 2(b) shows BFO nanorings with 80 nm of wall thickness patterned on Pt, which can serve as a bottom electrode for ferroelectric property measurement. BiFeO<sub>3</sub> nanolines with 80 nm of linewidth patterned on single crystalline (100) SrTiO<sub>3</sub> (STO) are shown in Fig. 2(c). SrTiO<sub>3</sub> is also a technologically important substrate (especially for perovskite structured materials) to be grown with highly textured or epitaxial structure. It is observed that the unpatterned area was well lifted off and all patterns main-

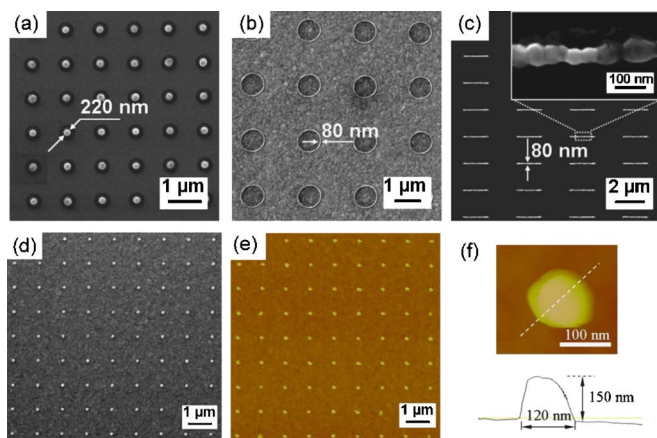


FIG. 2. (Color online) Microscopic characterization of BiFeO<sub>3</sub> nanopatterns on various substrates: scanning electron microscopy secondary electron images of (a) nanodots on Si, (b) nanorings on Pt, and (c) nanolines on (100) SrTiO<sub>3</sub>. (d) Nanodots with a diameter of about 100 nm patterned on Pt along with (e) tapping mode AFM images of the sample that was also used for ferroelectric property measurement, and (f) higher magnification image and the cross-section profile of a single dot.

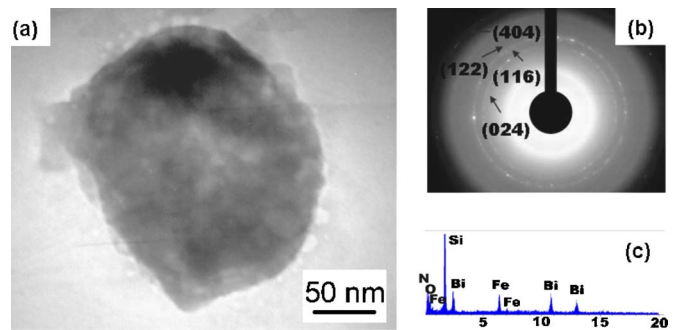


FIG. 3. (Color online) (a) Transmission electron microscopy image of a BiFeO<sub>3</sub> nanodot on SiN<sub>x</sub> membrane, (b) SAD pattern taken from the nanodot, and (c) energy dispersive spectrum obtained from the nanodot.

tained good uniformity in size and shape after heat treatment. Figures 2(d) and 2(e) show SEM and tapping mode AFM images of BFO dots of 120 nm in diameter and 150 nm in height patterned on Pt. This sample was used for the ferroelectric property measurement as will be described later. High-magnification images of one such BFO dot and its cross sectional profile are shown in Fig. 2(f). The SEM and AFM images reveal the capability of soft-eBL to fabricate solid structure with a dimension of less than 100 nm. These results also demonstrate the advantages of the soft-eBL technique as a combination of eBL and spin coating of the liquid-phase precursor. Soft-eBL inherits all the advantages of eBL, such as high patterning resolution due to the short wavelength of electron beam and flexible design of pattern shape and size via computer aided design software, because no physical mask plates are required.

In particular, the BFO nanolines patterned on STO exhibit a “bamboo” structure, with the linewidth approaching the single-grain dimension [as shown in the inset of Fig. 2(c)]. It is well known that one of the major limitations of BFO is the high leakage current.<sup>17,18</sup> Although oxygen vacancy is believed to be the origin of high conductivity,<sup>19,20</sup> the contribution of impurity and structure defects, normally agglomerating in grain boundary, should not be ignored. Such a pattern contains a well-controlled grain boundary structure and thus serves as a model system for investigating the role of grain boundary in the leakage problem associated with BFO.

BiFeO<sub>3</sub> was also patterned on an electron-transparent SiN<sub>x</sub> membrane window (thickness: 50 nm) for direct observation under transmission electron microscopy (TEM) (Hitachi 8100, Japan). Figure 3(a) shows the TEM image of a BFO nanodot. The corresponding selected area diffraction (SAD) pattern taken from this dot and shown in Fig. 3(b) indicates the polycrystalline feature of the as-prepared BFO nanodot. The measured diameters of the SAD rings correspond well to the lattice spacing of rhombohedrally structured BFO. The chemical constituents of the BFO patterns were confirmed by the energy dispersive spectrum obtained from these nanodots [Fig. 3(c)]. The signal of Si and N were generated by the membrane.

Piezoresponse force microscopy (PFM) was carried out in order to probe the ferroelectric behavior of the BFO nanopatterns. Piezoresponse force microscopy is a versatile technique, capable of not only domain structure imaging but also local hysteresis loop measurement. In this work, PFM was performed on BFO nanodots [SEM and AFM images shown in Figs. 2(d)–2(f)] using a Nanoscope IV-Dimension 3100

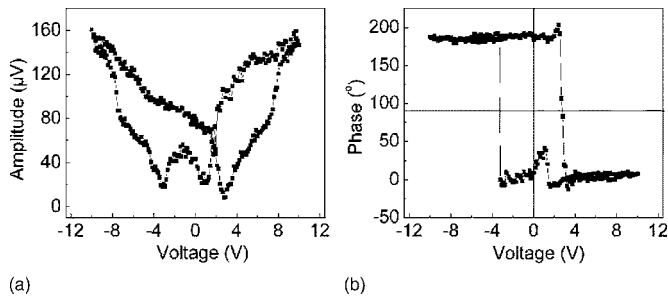


FIG. 4. Piezoresponse (a) amplitude and (b) phase loops measured at room temperature for a 100 nm BiFeO<sub>3</sub> nanodot patterned on Pt using PFM.

AFM (Digital Instrument, USA) equipped with a signal access module and an external lock-in amplifier (Signal Recovery Model 5210). Pt/Ti-coated conductive AFM probes (NSC18, MikroMasch, USA), having a nominal force constant of 3 N/m, were used. In our experiment, a 5 kHz ac electric field plus a swept dc voltage was applied to an individual dot via the tip. Figures 4(a) and 4(b) show the typical loops of piezoresponse amplitude and phase versus the applied voltage, respectively. The amplitude loop displays a butterfly shape, which is typical for ferroelectric materials. Meanwhile, as the voltage changes from about +3 to -3 V, the 180° phase change indicates an unambiguous ferroelectric switch. Consider the height of the nanodot is about 150 nm, the specific coercive field is about 20 MV/m, close to the values published for BFO epitaxial thin films.<sup>8,21</sup> These collective results validate the ferroelectric characteristics of the BFO nanopatterns.

Magnetic hysteresis loop was determined at room temperature by using a superconducting quantum interference device magnetometer (MPSM-5, Quantum design, USA) and applying an out-of-plane magnetic field. In order to generate detectable signal, a large area of BFO patterns with a diameter of 1 μm was fabricated on platinized silicon substrate. The total number of the pattern elements is about  $1.6 \times 10^6$ . Figure 5 shows the hysteresis loop, which reveals a saturation magnetization of about 10 emu/cm<sup>3</sup> in the magnetic field larger than 1000 Oe. BiFeO<sub>3</sub> is a G-type antiferromagnetic material which means that the spins in the adjacent Fe atoms are antiparallel.<sup>8,22,23</sup> On the other hand, the spin canting effect allows BFO to possess a weak macroscopic magnetization.<sup>24</sup> Therefore, the hysteresis loop of BFO patterns does not show obvious remnant magnetization and coercive field. These results are consistent with the data already published for BFO thin films<sup>8,18,25</sup> and thereby confirmed the multiferroic behavior of the BFO nanopatterns by soft-eBL.

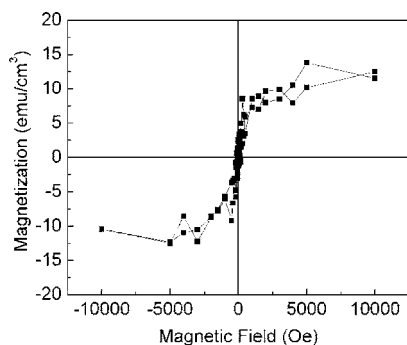


FIG. 5. Magnetic hysteresis loop measured at room temperature for BiFeO<sub>3</sub> dots (1 μm in diameter) patterned on Pt.

In summary, multiferroic BFO nanopatterns with defined shape, size, and separation were fabricated on diverse substrates using the soft-eBL technique. The coexistence of ferroelectric and ferromagnetic behavior at room temperature was demonstrated by PFM and the magnetic hysteresis loop, respectively. In addition, the BFO nanolines patterned on single crystal (100) STO substrate exhibit an interesting bamboo-like microstructure that may prove useful in elucidating the role of grain boundaries on leakage current in BFO. The ability to fabricate multiferroic nanostructures not only opens an avenue for designing high-performance devices but also enables investigation of the size effect on multiferroic phenomena.

This work was partially supported by the U.S. Department of Energy under Contract No. W-31-109-ENG-38, NSF-NSEC under Contract No. EEC-0118025/003 and NSF-MRSEC under Contract No. DMR-0520513. The research work was performed in the EPIC and NIFTI facilities of the NUANCE Center at Northwestern University. The NUANCE Center is supported by NSF-NSEC, NSF-MRSEC, the State of Illinois, and Northwestern University.

- <sup>1</sup>Z. H. Zhong, D. L. Wang, Y. Cui, M. W. Bockrath, and C. M. Lieber, *Science* **302**, 1377 (2003).
- <sup>2</sup>Z. L. Wang and J. H. Song, *Science* **312**, 242 (2006).
- <sup>3</sup>N. Hur, S. Park, P. A. Sharma, J. S. Ahn, S. Guha, and S. W. Cheong, *Nature (London)* **429**, 392 (2004).
- <sup>4</sup>T. Kimura, T. Goto, H. Shintani, K. Ishizaka, T. Arima, and Y. Tokura, *Nature (London)* **426**, 55 (2003).
- <sup>5</sup>M. Fiebig, T. Lottermoser, D. Frohlich, A. V. Goitsev, and R. V. Pisarev, *Nature (London)* **419**, 818 (2002).
- <sup>6</sup>G. A. Smolenskii, V. M. Yudin, E. S. Sher, and Y. E. Stolypin, *Sov. Phys. JETP* **16**, 622 (1963).
- <sup>7</sup>C. Michel, J. M. Moreau, G. D. Achenbac, R. Gerson, and W. J. James, *Solid State Commun.* **7**, 701 (1969).
- <sup>8</sup>J. Wang, J. B. Neaton, H. Zheng, V. Nagarajan, S. B. Ogale, B. Liu, D. Viehland, V. Vaithyanathan, D. G. Schlom, U. V. Waghmare, N. A. Spaldin, K. M. Rabe, M. Wuttig, and R. Ramesh, *Science* **299**, 1719 (2003).
- <sup>9</sup>K. Y. Yun, D. Ricinchi, T. Kanashima, M. Noda, and M. Okuyama, *Jpn. J. Appl. Phys., Part 2* **43**, L647 (2004).
- <sup>10</sup>F. M. Bai, J. L. Wang, M. Wuttig, J. F. Li, N. G. Wang, A. P. Pyatakov, A. K. Zvezdin, L. E. Cross, and D. Viehland, *Appl. Phys. Lett.* **86**, 032511 (2005).
- <sup>11</sup>V. Nagarajan, A. Roytburd, A. Stanishevsky, S. Prasertchoung, T. Zhao, L. Chen, J. Melngailis, O. Auciello, and R. Ramesh, *Nat. Mater.* **2**, 43 (2003).
- <sup>12</sup>A. L. Roytburd, S. P. Alpay, V. Nagarajan, C. S. Ganpule, S. Aggarwal, E. D. Williams, and R. Ramesh, *Phys. Rev. Lett.* **85**, 190 (2000).
- <sup>13</sup>X. Y. Zhang, C. W. Lai, X. Zhao, D. Y. Wang, and J. Y. Dai, *Appl. Phys. Lett.* **87**, 143102 (2005).
- <sup>14</sup>T. J. Park, Y. B. Mao, and S. S. Wong, *Chem. Commun. (Cambridge)* **2004**, 2708.
- <sup>15</sup>S. Donthu, Z. X. Pan, B. Myers, G. Shekhawat, N. G. Wu, and V. Dravid, *Nano Lett.* **5**, 1710 (2005).
- <sup>16</sup>Z. X. Pan, S. K. Donthu, N. Q. Wu, S. Y. Li, and V. P. Dravid, *Small* **2**, 274 (2006).
- <sup>17</sup>C. F. Chung and J. M. Wu, *Electrochem. Solid-State Lett.* **8**, F63 (2005).
- <sup>18</sup>D. Lee, M. G. Kim, S. Ryu, H. M. Jang, and S. G. Lee, *Appl. Phys. Lett.* **86**, 222903 (2005).
- <sup>19</sup>H. Uchida, R. Ueno, H. Nakaki, H. Funakubo, and S. Koda, *Jpn. J. Appl. Phys., Part 2* **44**, L561 (2005).
- <sup>20</sup>J. K. Kim, S. S. Kim, W. J. Kim, A. S. Bhalla, and R. Guo, *Appl. Phys. Lett.* **88**, 132901 (2006).
- <sup>21</sup>S. Y. Yang, F. Zavaliche, L. M. Ardabili, V. Vaithyanathan, D. G. Schlom, Y. J. Lee, Y. H. Chu, M. P. Cruz, Q. Zhan, T. Zhao, and R. Ramesh, *Appl. Phys. Lett.* **87**, 102903 (2005).
- <sup>22</sup>B. Ruetter, S. Zvyagin, A. P. Pyatakov, A. Bush, J. F. Li, V. I. Belotelov, A. K. Zvezdin, and D. Viehland, *Phys. Rev. B* **69**, 064114 (2004).
- <sup>23</sup>C. Ederer and N. A. Spaldin, *Phys. Rev. B* **71**, 224103 (2005).
- <sup>24</sup>C. Ederer and N. A. Spaldin, *Phys. Rev. B* **71**, 060401 (2005).
- <sup>25</sup>Y. H. Lee, J. M. Wu, and C. H. Lai, *Appl. Phys. Lett.* **88**, 042903 (2006).